Lattice Boltzmann method for oscillatory Stokes flow with applications to micro- and nanodevices

Yong Shi[1,2] and John E. Sader[2,*]
[1]*School of Power Engineering, Chongqing University, Chongqing 400030, People's Republic of China*
[2]*Department of Mathematics and Statistics, University of Melbourne, Victoria 3010, Australia*
(Received 11 January 2010; published 22 March 2010)

A lattice Boltzmann (LB) method based on the linearized Boltzmann Bhatnagar-Gross-Krook equation for numerical simulation of oscillatory (unsteady) Stokes flow is proposed. Unlike the conventional (nonlinear) LB method that utilizes the time domain exclusively, the proposed method is formulated in the frequency domain to allow for direct access to the complex-valued stress, force, and velocity field—these parameters are of direct interest in characterizing microelectromechanical systems (MEMS) and nanoelectromechanical systems (NEMS). The proposed method circumvents the requirement for time-dependent boundary velocities, as is needed in the conventional LB method, and convergence of the two methods is compared. Validity of the proposed method is assessed using three classical (unsteady) flows: (1) *one-dimensional* oscillatory Couette flow between two plates; (2) *two-dimensional* flow generated by an oscillating circular cylinder; (3) *three-dimensional* flow generated by an oscillating sphere. The observed excellent numerical performance in all three cases demonstrates that this linear lattice Boltzmann method can be used to study the dynamics of micro- and nanoscale devices of any dimensionality. This is particularly relevant to MEMS and NEMS, where the resonance properties of individual nanomechanical components immersed in fluid can underpin overall device performance.

DOI: 10.1103/PhysRevE.81.036706 PACS number(s): 47.11.−j, 47.61.−k

I. INTRODUCTION

The lattice Boltzmann (LB) method is an established approach for computational fluid dynamics, which has shown increasing utility in recent years [1–4]. In contrast to conventional numerical methods that simulate flows based on (macroscopic) conservation laws, the LB method numerically solves the kinetic equation for the (mesoscopic) particle distribution function [5–7]. Such a kinetic basis leads to a number of distinct advantages in comparison to conventional numerical methods, which include a natural capacity to incorporate microscopic physical laws [6,8,9], intrinsic accommodation of complex-shaped boundaries [10–12], a fully parallel computational structure [13,14], and all while utilizing a simple numerical algorithm [4]. The lattice Boltzmann method, as an alternative and reliable numerical scheme, is now being used to simulate a wide range of fluid transport phenomena, such as turbulent flow [15,16], flow through porous media [17,18], multiphase flows [19,20], magnetohydrodynamics [21], suspension flows [22,23], and biofluid flows [24,25]. Moreover, in very recent years, it has been further developed as a multifunctional numerical tool for modeling of multiphysical transport process far beyond fluid dynamics [4,26–28].

The LB method was originally developed from the lattice-gas cellular automata (LGCA), which mimics real particle dynamics at the microscale as a simplified streaming-collision procedure of virtual representative particles on a regular lattice [29]. As early as 1986, the LGCA method was demonstrated to numerically simulate fluid flow at Navier-Stokes order in two dimensions, provided a triangular lattice with hexagonal symmetry and a well-designed collision procedure were used [30]. However, the method was found to always suffer from statistical noise. This was overcome by McNamara and Zanetti [31] who proposed that the Boolean occupation number in the LGCA method should be replaced by a floating-digital distribution function and use be made of the ensemble average. This improvement gave birth to the first generation of LB models [31–33]. The LB method gained wide acceptance as an alternative and accurate numerical approach following the work of Chen *et al.* [21] and Qian *et al.* [34], who simplified local particle collisions using the Bhatnagar-Gross-Krook (BGK) relaxation approximation and hence derived a BGK model of the LB method. In comparison to the original LGCA model, this BGK LB model exhibits a simplified formulation and successfully removes many intrinsic drawbacks of the LGCA method, including violation of Galilean invariance and pressure dependence on the velocity [29].

It should also be noted that the LB method has a direct link to the kinetic theory of gases. He and Luo [5] demonstrated that many commonly used LB models can be constructed by (i) directly discretizing the Boltzmann BGK equation using conventional finite difference techniques, (ii) expanding the Maxwellian distribution in its Taylor series up to second order in Mach number, and (iii) evaluating the corresponding moments with Gaussian-Hermite quadrature in the continuum limit. Importantly, it can be shown that the LB method exactly recovers the complete Navier-Stokes equations through the Chapman-Enskog procedure. Therefore, while the Boltzmann BGK equation is used widely in rarefied gas dynamics calculations, the corresponding discrete LB BGK method provides a robust numerical scheme for directly solving continuum flows, regardless of the nature of the fluid (gas or liquid).

In very recent years, burgeoning development in microfabrication technologies and nanoscience has triggered new

*Author to whom correspondence should be addressed; jsader@unimelb.edu.au

interest in the LB method. A wide variety of studies [35–37] have applied the LB method to investigate micro- and nanoscale fluid dynamics, since fluid transport in small structures often has a significant impact on device performance and efficiency. Generally, for most liquid flows and some gas flows [38,39] at small length scales, the classical Navier-Stokes equations with the no-slip boundary condition are a valid mathematical description. We thus focus on continuum flows throughout and ignore any higher-order effects due to finite molecular size. On the other hand, micro- and nanoscale flow dynamics also present many features distinct from that at the macroscale. For example, fluid flows (both liquid and gas) in small structures have an almost negligible Reynolds number, $\mathrm{Re}=uL/\nu$, with u, L, and ν being the characteristic velocity scale, characteristic flow length scale, and kinematic viscosity of the fluid, respectively. This immediately indicates that the nonlinear advective inertial force is negligibly small in the Navier-Stokes equations and therefore micro- and nanoscale flow dynamics can be well described by the linearized Navier-Stokes equations; also commonly referred to as the "unsteady Stokes equations."

While flows generated by oscillating micro- and nanostructures are in general linear, their numerical computation presents a challenging task nonetheless. Such structures often exhibit complicated geometries and involve periodically deforming components, e.g., accelerometers, cantilever devices, resonant sensors, and microengines [39–42]. Several limitations are thus found when the conventional time-dependent LB method is applied:

(1) The conventional LB method is constructed based on the nonlinear Boltzmann BGK equation [5]. Macroscopically, this is equivalent to solving the full Navier-Stokes equations, complete with the usual nonlinear advective inertial term. This inherent nonlinearity is insignificant in many small-scale flows and adds a level of complexity that is normally not required.

(2) As an explicit time-marching scheme, the conventional LB method numerically solves the distribution function in the time domain. A very small time step in comparison to the characteristic time of flows is thus adopted to ensure sufficient accuracy. Such a treatment inevitably results in computationally inefficiencies for some unsteady flows, e.g., oscillatory flows, where many periods of oscillation must be simulated to extract information on the steady-state behavior of a single period at "long time."

(3) Due to oscillatory motion, the conventional LB method must update and reset boundary conditions at the interface between the fluid and the solid oscillating bodies at every time step. This can be computationally expensive and necessitates significant extra coding, particularly when the oscillating bodies have complex geometries.

Importantly, the response of an oscillating mechanical structure in contact with fluid is most commonly measured in the frequency domain rather than in the time domain. While these two treatments are equivalent and complementary, measurement of the frequency response yields a more natural and accurate result and is used widely in characterizing device performance. This is particularly significant in applications and development in microelectromechanical systems (MEMS) and nanoelectromechanical systems (NEMS), where resonating structures in fluid often appear [43–45].

This motivates development of a linear lattice Boltzmann method in the frequency domain for oscillatory flows, whose output can be directly compared to experimental data and used in device development. The complete oscillatory flow is then solved on a fixed boundary in the frequency domain, thus dramatically simplifying implementation. We also note that a transient time response can always be obtained from calculation in the frequency domain using the inverse Fourier transform.

Unlike previous lattice Boltzmann methods, the proposed linear frequency-domain LB method is formulated by (i) derivation of a complex relaxation time λ^* and (ii) introduction of a virtual time τ. The latter feature ensures that the proposed method retains the time-marching algorithmic structure of the conventional lattice Boltzmann method. As such, this enables trivial implementation of the proposed LB method into many existing lattice Boltzmann programs, without major modification. We again emphasize that the proposed LB method is developed for general continuum flows and holds for both gases and liquids, the reasons of which are discussed above.

The paper is organized as follows. The linearized Boltzmann BGK equation is first reviewed in Sec. II. Formulation of the LB method in the frequency domain is then derived in Sec. III. In Sec. IV, the proposed method is validated using three classical oscillatory flow problems, ranging from one dimensional to three dimensional in nature. Computational convergence of the proposed LB method in comparison to the conventional time-dependent lattice Boltzmann method is also examined. Additional theoretical discussion of the macroscopic equations derived from the proposed LB method is relegated to Appendixes A and B, along with exact solutions to the three classical flow problems studied in Sec. IV.

II. LINEARIZED BOLTZMANN BGK EQUATION

The Boltzmann BGK equation [46] can be directly used to simulate continuum flows

$$\frac{\partial f}{\partial t}+\mathbf{c}\cdot\frac{\partial f}{\partial \mathbf{r}}=-\frac{1}{\lambda}(f-f^{eq}), \tag{1}$$

where f is the distribution function, whereas t, $\mathbf{r}$, $\mathbf{c}$, and λ are the time, particle position, particle velocity, and relaxation time, respectively. The local equilibrium distribution function, f^{eq}, is given by

$$f^{eq}=\frac{\rho(\mathbf{r},t)}{(2\pi RT_0)^{D/2}}\exp\left\{-\frac{[\mathbf{c}-\mathbf{u}(\mathbf{r},t)]^2}{2RT_0}\right\}, \tag{2}$$

where D is the dimensionality of the flow, R is the gas constant, T_0 is the absolute temperature at equilibrium, and ρ and $\mathbf{u}$ are the fluid density and velocity, respectively, which are defined as

$$\rho=\int f d\mathbf{c}, \quad \rho\mathbf{u}=\int f\mathbf{c}d\mathbf{c}, \tag{3}$$

where $\int\ldots d\mathbf{c}$ denotes volume integration over all velocity space [47]. In this paper, we only study isothermal flows so

that the fluid temperature is constant, i.e., $T=T_0$. Importantly, using the Chapman-Enskog procedure [47], the Boltzmann BGK equation, Eq. (1), can be shown to exactly recover the Navier-Stokes equations with the nonlinear advective inertial force in the continuum limit. It is our aim to develop a frequency-domain LB method for linear flows and thus require that this nonlinearity be eliminated.

The inherent nonlinearity in the Boltzmann BGK equation, Eq. (1), can be removed through appropriate linearization. Suppose that the fluid system is perturbed from its global equilibrium at constant density ρ_0 and zero velocity, i.e., $\boldsymbol{u}_0=\mathbf{0}$. Such a perturbation is assumed to be infinitesimally small and quantified by

$$h = \frac{f}{\bar{f}^{eq}} - 1, \tag{4}$$

where $\bar{f}^{eq}$ is the global equilibrium given by

$$\bar{f}^{eq} = \frac{\rho_0}{(2\pi RT_0)^{D/2}} \exp\left(-\frac{\mathbf{c}^2}{2RT_0}\right). \tag{5}$$

Perturbations to the fluid density and velocity, i.e., $\delta\rho$ and $\delta\mathbf{u}$, are then given by the moments of h, which are

$$\delta\rho = \int \bar{f}^{eq} h d\mathbf{c} \tag{6}$$

and

$$\rho_0 \delta\mathbf{u} = \rho_0 \mathbf{u} = \int \bar{f}^{eq} h \mathbf{c} d\mathbf{c}. \tag{7}$$

Next, we expand the local equilibrium distribution, f^{eq}, using its Taylor series about the global equilibrium, $\bar{f}^{eq}$. Neglecting all the high-order nonlinear terms in the expansion, we obtain the linearized form

$$f_L^{eq} = \bar{f}^{eq}\left(1 + \frac{\delta\rho}{\rho_0} + \frac{\mathbf{c}\cdot\mathbf{u}}{RT_0}\right). \tag{8}$$

Moreover, the equilibrium of h can also be derived, yielding

$$h^{eq} = \frac{f_L^{eq}}{\bar{f}^{eq}} - 1 = \frac{\delta\rho}{\rho_0} + \frac{\mathbf{c}\cdot\mathbf{u}}{RT_0}. \tag{9}$$

With the help of Eqs. (4)–(8), we readily derive a linear kinetic equation for h from Eq. (1) [48]

$$\frac{\partial h}{\partial t} + \mathbf{c}\cdot\frac{\partial h}{\partial \mathbf{r}} = -\frac{h}{\lambda} + \frac{1}{\lambda\theta^{D/2}}\int \exp\left(-\frac{\mathbf{c}^2}{2RT_0}\right) h d\mathbf{c} + \frac{1}{\lambda\theta^{D/2}}\frac{\mathbf{c}}{RT_0}\cdot\int \exp\left(-\frac{\mathbf{c}^2}{2RT_0}\right) h\mathbf{c} d\mathbf{c}, \tag{10}$$

where $\theta=2\pi RT_0$. Using Eqs. (6) and (7), Eq. (10) then becomes

$$\frac{\partial h}{\partial t} + \mathbf{c}\cdot\frac{\partial h}{\partial \mathbf{r}} = -\frac{h}{\lambda} + \frac{1}{\lambda}\frac{\delta\rho}{\rho_0} + \frac{1}{\lambda}\frac{\mathbf{c}\cdot\mathbf{u}}{RT_0}. \tag{11}$$

Equation (10) [or Eq. (11)] is the well-known linearized Boltzmann BGK equation. It is valid for flows in the entire range of the Knudsen number (defined as the ratio of the molecular dimension to the macroscopic length scale) provided that the flow perturbation from the global equilibrium is very small. Furthermore, using the Chapman-Enskog procedure, it can be proved that the linearized Navier-Stokes equations are recovered from Eq. (10) in the continuum limit (see Appendix A). Analytical solution of Eq. (10) presents a formidable challenge, except for the simplest of flows [48]. In the next section, we develop a robust and tractable lattice Boltzmann algorithm based on Eq. (10).

III. LINEAR LATTICE BOLTZMANN METHOD

A. Discrete-velocity linearized Boltzmann BGK equation

The first step in constructing a linear LB method is to discretize the particle velocity space of Eq. (10). It should be emphasized that our aim is to develop a linear LB method for unsteady Stokes flow, i.e., in the continuum limit. Therefore, all relevant moments over continuous particle velocity space must be *exactly* evaluated by quadratures based on the proposed finite discrete particle velocities in order to recover the linearized Navier-Stokes equations from Eq. (10). As shown in Appendix A, we need to exactly compute the following moments weighed by $\exp[-\mathbf{c}^2/(2RT_0)]$:

conservation of mass:

$$1, \quad c_\alpha, \quad c_\alpha c_\beta, \quad c_\alpha c_\beta c_\gamma, \tag{12}$$

conservation of momentum:

$$c_\alpha, \quad c_\alpha c_\beta, \quad c_\alpha c_\beta c_\gamma, \quad c_\alpha c_\beta c_\gamma c_\eta, \tag{13}$$

where c_α is the α component of the particle velocity $\mathbf{c}$ in the Cartesian frame. The moments in Eqs. (12) and (13) are at most fourth order, establishing that the discrete-velocity sets for the conventional nonlinear lattice Boltzmann method [34] are also valid for the present linear version. For *two-dimensional* flows, we have the 9-bit set

$$\mathbf{c}_j = \begin{cases} (0,0), & j=0 \\ c(\cos[(j-1)\pi/2],\ \sin[(j-1)\pi/2]), & j=1,2,3,4 \\ \sqrt{2}c\ (\cos[(2j-9)\pi/4],\ \sin[(2j-9)\pi/4]), & j=5,6,7,8, \end{cases} \tag{14}$$

while the 15-bit set for *three-dimensional* flows is

$$\mathbf{c}_j = \begin{cases} (0,0,0), & j=0 \\ c(\pm 1,0,0), c(0,\pm 1,0), c(0,0,\pm 1), & j=1,2,\ldots,6 \\ c(\pm 1,\pm 1,\pm 1), & j=7,8,\ldots,14, \end{cases} \tag{15}$$

where the speed $c=\sqrt{3RT_0}$. With the discrete velocities given in Eq. (14) and (15), the linearized Boltzmann BGK equation, Eq. (10), can be rewritten in its discrete-velocity form

$$\frac{\partial h_j}{\partial t} + \mathbf{c}_j \cdot \frac{\partial h_j}{\partial \mathbf{r}} = -\frac{1}{\lambda}(h_j - h_j^{eq}), \tag{16}$$

where h_j is the deviation of the distribution function defined in Eq. (4), in terms of the velocity $\mathbf{c}_j$, and h_j^{eq} is its equilibrium distribution given by

$$h_j^{eq} = \frac{\delta\rho}{\rho_0} + \frac{\mathbf{c}_j \cdot \mathbf{u}}{RT_0}, \tag{17}$$

with

$$\delta\rho = \rho_0 \sum_j w_j h_j, \tag{18}$$

$$\mathbf{u} = \sum_j w_j h_j \mathbf{c}_j, \tag{19}$$

and w_j is the weight corresponding to the jth discrete particle velocity. For the two-dimensional 9-bit set, we have

$$w_j = \begin{cases} 4/9, & j=0 \\ 1/9, & j=1,2,3,4 \\ 1/36, & j=5,6,7,8, \end{cases} \tag{20}$$

while for the three-dimensional 15-bit set,

$$w_j = \begin{cases} 2/9, & j=0 \\ 1/9, & j=1,2,\ldots,6 \\ 1/72, & j=7,8,\ldots,14. \end{cases} \tag{21}$$

B. Linear frequency-domain lattice Boltzmann model

Conventionally, the next step in constructing a lattice Boltzmann model is to further discretize physical space and time in Eq. (16). However, here we shall construct an alternative linear lattice Boltzmann method for oscillatory flows in the frequency domain rather than the time domain. To this end, we first re-express all dependent variables (denoted ψ) in terms of the explicit time dependence $e^{i\omega t}$, such that

$$\psi(\boldsymbol{r},\boldsymbol{c},t) = \hat{\psi}(\boldsymbol{r},\boldsymbol{c}|\omega)e^{i\omega t}, \tag{22}$$

where ω and i are the radial frequency and the usual imaginary unit, respectively. With Eq. (22), we derive a new Boltzmann BGK equation in the frequency domain from the discrete-velocity linearized Boltzmann BGK equation, Eq. (16), which is

$$\mathbf{c}_j \cdot \frac{\partial \hat{h}_j}{\partial \mathbf{r}} = -\frac{\hat{h}_j}{\lambda^*} + \frac{\hat{h}_j^{eq}}{\lambda}, \tag{23}$$

where $\lambda^* = \lambda/(1+i\omega\lambda)$ and the equilibrium distribution is

$$\hat{h}_j^{eq} = \frac{\delta\hat{\rho}}{\rho_0} + \frac{\mathbf{c}_j \cdot \hat{\mathbf{u}}}{RT_0}, \tag{24}$$

with

$$\delta\hat{\rho} = \rho_0 \sum_j w_j \hat{h}_j, \tag{25}$$

$$\hat{\mathbf{u}} = \sum_j w_j \hat{h}_j \mathbf{c}_j. \tag{26}$$

Note that Eq. (23) is independent of time t and the original time derivative of h_j in Eq. (16) has been transformed into the product of $\hat{h}_j$ and $i\omega$, which is absorbed into the complex relaxation time λ^*.

Mathematically, Eq. (23) can be regarded as a steady-state Boltzmann BGK equation with a newly defined complex relaxation time λ^*. As such, the left-hand side of Eq. (23) can be formally identified as the *material derivative* of $\hat{h}_j$ for a time-independent problem. Introducing a "virtual time," τ, into the left-hand side of Eq. (23) then leads to a (virtual) time-dependent discrete-velocity Boltzmann BGK equation in the frequency domain

$$\frac{D\hat{h}_j}{D\tau} \equiv \frac{\partial \hat{h}_j}{\partial \tau} + \mathbf{c}_j \cdot \frac{\partial \hat{h}_j}{\partial \mathbf{r}} = -\frac{\hat{h}_j}{\lambda^*} + \frac{\hat{h}_j^{eq}}{\lambda}, \tag{27}$$

where $D\hat{h}_j/D\tau$ is the material derivative of $\hat{h}_j$ with respect to virtual time τ. Clearly, the steady-state solution to Eq. (27) is the solution to Eq. (23). Introduction of the material derivative in Eq. (27) is important since it establishes that the original explicit time-marching lattice Boltzmann algorithm for the transient Boltzmann BGK equation can be used to solve Eq. (23) in the frequency domain. Consequently, all existing lattice Boltzmann programs can be readily modified to accommodate linear frequency-domain calculations, requiring only slight modifications to the relaxation time and equilibrium distribution.

Based on this formulation, we discretize virtual time and physical space in Eq. (27). The linear lattice Boltzmann equation in the frequency domain is then obtained

$$\hat{h}_j(\mathbf{r}+\mathbf{c}_j\Delta\tau,\tau+\Delta\tau) - \hat{h}_j(\mathbf{r},\tau) = -\Omega^*\hat{h}_j(\mathbf{r},\tau) + \Omega\hat{h}_j^{eq}(\mathbf{r},\tau) - \frac{\Delta\tau^2}{2}\omega^2\hat{h}_j^{eq}(\mathbf{r},\tau), \tag{28}$$

where $\Delta\tau$ is the virtual time step, the dimensionless complex relaxation frequency is $\Omega^* = \Delta\tau/\lambda^*$, and the dimensionless relaxation frequency is $\Omega = \Delta\tau/\lambda$. Using the Chapman-Enskog procedure, it can be proved that the linearized Navier-Stokes equations in the frequency domain are recovered in the steady-state limit of Eq. (28) (see Appendix B). It should be also pointed out that the above proposed LB

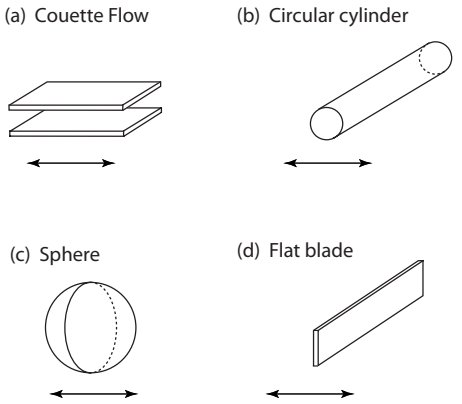

FIG. 1. Four linear oscillatory flows. (a) One-dimensional oscillatory Couette flow. (b) Two-dimensional flow around an oscillating circular cylinder. (c) Three-dimensional flow around an oscillating sphere. (d) Two-dimensional flow generated by an oscillating (infinitely thin) flat blade.

method is strictly valid in the incompressible limit, even though it uses compressible state variables; this feature is true for all LB models. The proposed LB model is thus a weakly compressible scheme for linear incompressible flows and the incompressible limit is implicitly used throughout this paper. Furthermore, in comparison to Eq. (27), Eq. (28) includes an addition term of order of $\Delta\tau^2$ on the right side. This is a discrete correction, which ensures that the proposed lattice Boltzmann method achieves second-order accuracy for unsteady Stokes flows, i.e., in the continuum limit.

In summary, we have developed a linear lattice Boltzmann method in the frequency domain, which consists of (i) an evolution equation, Eq. (28), (ii) the local equilibrium, Eq. (24), (iii) discrete-velocity sets for two-dimensional flows in Eq. (14) and three-dimensional flows in Eq. (15), and (iv) commensurate quadratures for the macroscopic flow variables in Eqs. (25) and (26), respectively. As with the conventional LB method, this proposed LB method can be numerically implemented as an explicit time-marching scheme. The "steady-state" results obtained by Eq. (28) then give the unsteady Stokes flow solution in the frequency domain.

IV. NUMERICAL SIMULATIONS AND DISCUSSION

In this section, we first validate the proposed linear lattice Boltzmann method using a series of classical flows, which range from one to three dimensional in nature. These are (i) oscillatory Couette flow between two planar walls [see Fig. 1(a)], (ii) two-dimensional flow around an oscillating circular cylinder [see Fig. 1(b)], and (iii) three-dimensional flow around an oscillating sphere [see Fig. 1(c)]. We then compare the numerical convergence of the proposed method to the conventional LB method based on simulations of the two-dimensional flow generated by an oscillating flat blade [see Fig. 1(d)].

We emphasize that the proposed LB method is implemented on fixed spatial domains, eliminating any need for time-dependent boundary reconstruction. This is in direct contrast to the requirements for conventional LB solutions of oscillatory flows generated by moving boundaries, as discussed above.

A. Validations

1. One-dimensional oscillatory Couette flow

We first apply the proposed LB method to simulate one-dimensional oscillatory Couette flow. Consider a viscous fluid of density ρ and kinematic viscosity ν that is confined between two parallel plates, which are separated by a distance L. Here, the top plate is stationary while the bottom plate oscillates in its own plane with a velocity $u=u_0e^{i\omega t}$, where u_0 is a constant and ω is the radial frequency. The no-slip boundary condition is applied to the fluid in contact with the two plates and the Stokes parameter characterizing flow behavior is defined $\beta=L^2\omega/\nu$.

Equation (14), together with Eq. (20), was chosen as the underlying discrete-velocity set and corresponding weights for the lattice Boltzmann simulation. Periodic boundary conditions were applied to the inlet and outlet and the nonequilibrium extrapolation method [11] was used to prescribe the distribution functions on the solid plates based on the corresponding macroscopic no-slip boundary condition. To nondimensionalize the simulation, we set the distance of the plates $L=1$ and the reference density $\rho_0=1$; this is equivalent to scaling the original LB method. To obtain the shear stress on the oscillating plate, we evaluated the velocity gradient at the wall using the second-order upwind finite-difference scheme.

Numerical simulations were performed using a 200×200 mesh; finer meshes did not reveal any significant improvement in accuracy. Figure 2 presents the resulting dimensionless streamwise velocities $\hat{U}$ (i.e., velocity components parallel to the plates) for a range of Stokes parameters $\beta=5$, 25, 50, and 75. Note that the fluid velocity is a complex-valued function in the frequency domain and as such, consists of a real and imaginary component (see Fig. 2). Our results demonstrate that for flows with a small Stokes parameter, β, the entire fluid region is affected by motion of the bottom plate. This is expected since the distance between the plates is much smaller than the characteristic viscous penetration depth. For flows with large β, however, the flow exhibits different behavior. Two distinct flow regions are clearly observed in the domain between the plates: a thin region near the moving plate, where significant fluid motion is observed, and an outer region where the fluid is not significantly perturbed. This is in line with expectation, since the viscous penetration depth in this case is very small and the flow closely resembles that of Stokes second problem for the oscillation of a single plate in an unbounded fluid. Most significantly, in all flow regimes, we find that the simulation results closely follow the exact analytical solution, which is presented in Appendix C, Sec. C 1.

Another important flow parameter is the shear stress exerted by the fluid on the oscillating plate. Table I lists shear stresses obtained by the proposed LB method and the exact analytical solution for flows with different Stokes parameters, β. As was found for the fluid velocity, numerical results for the shear stress agree very well with the analytical

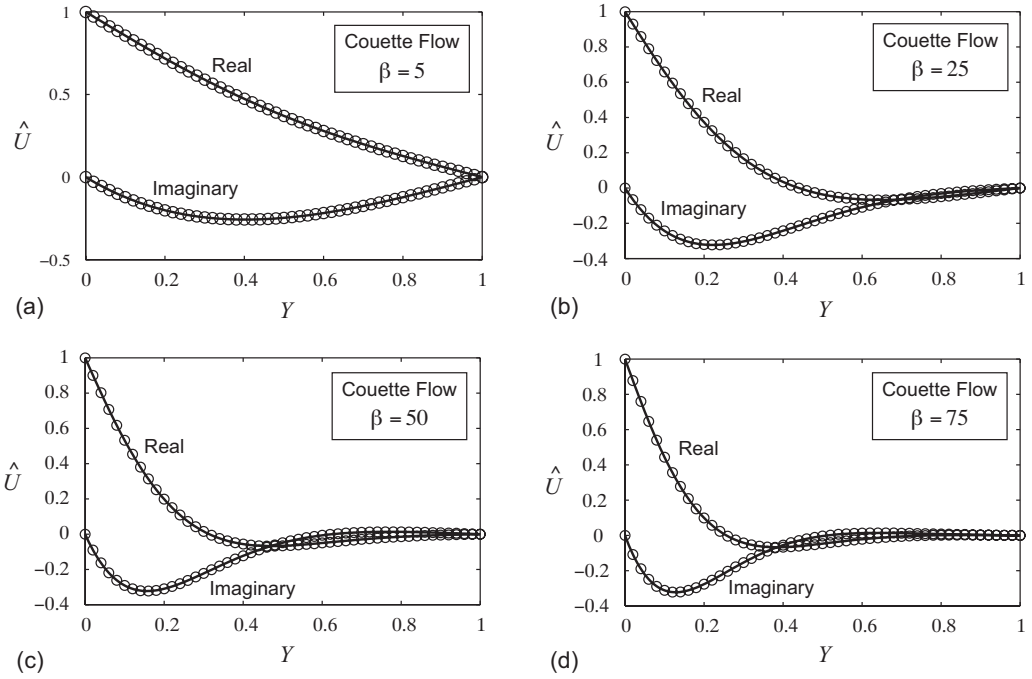

FIG. 2. Dimensionless streamwise velocities in one-dimensional oscillatory Couette flow. Open circles: numerical results; solid lines: analytical solution.

solution. This demonstrates that the proposed frequency-domain linear lattice Boltzmann method can capture all flow characteristics of this classical problem.

2. *Two-dimensional flow around an oscillating circular cylinder*

Next, we apply the proposed LB method to study the flow generated by an oscillating circular cylinder in an unbounded fluid. This classical two-dimensional flow problem was originally solved by Stokes in 1851, the exact solution of which is given in Appendix C. Sec. C 2 [49,50]. We consider a circular cylinder immersed in a viscous fluid that is oscillating perpendicular to its axis with a velocity $u=u_0e^{i\omega t}$. The fluid in contact with the surface of the cylinder satisfies the no-slip condition. We consider that the spatial amplitude of oscillation is much smaller than the cylinder radius, so that the flow is accurately described by the linearized Navier-Stokes equations; this assumption is implicitly assumed in this paper.

Since the flow is two dimensional, Eq. (14) is used as the discrete-velocity set for the lattice Boltzmann simulation of this flow. Further, to nondimensionalize the problem, we numerically set the radius of the cylinder $a=1$, the reference density $\rho_0=1$, and define the Stokes parameter $\beta=a^2\omega/\nu$. The computational domain was varied up to a size of $100a \times 100a$ to ensure the fluid velocity at the domain boundaries had decayed sufficiently and did not influence the simulation. As for the boundary conditions, the nonequilibrium extrapolation method [11] was applied to the outer boundaries of the computational domain while the bounce back-based interpolation method (BBIM) [12] was applied to the curved cylinder surface to ensure satisfaction of the no-slip condition. To evaluate the force exerted by the fluid on the cylinder, we employed the momentum exchange method [12]. This approach is used here since the force evaluation method in Sec. IV A 1 is computationally expensive and complicated for two-dimensional flows with curved boundaries; it is generally inapplicable to three-dimensional flows [51].

TABLE I. Dimensionless shear stress on the oscillating plate in one-dimensional oscillatory Couette flow.

	$\mathrm{Re}(\hat{F})$		$\mathrm{Im}(\hat{F})$	
$\beta=\omega L^2/\nu$	Numerical	Analytical	Numerical	Analytical
5	−0.2901	−0.2900	−0.2926	−0.2911
25	−0.1418	−0.1418	−0.1408	−0.1414
50	−0.1000	−0.1000	−0.1001	−0.1000
75	−0.0816	−0.0817	−0.0805	−0.0817

The computational domain of $100a \times 100a$ was discretized using a 700×700 mesh for the following Stokes parameters $\beta=1$, 5, and 10. Second-order interpolation was used in the BBIM for the flow with $\beta=10$ while first-order interpolation was adopted for all other cases (with smaller Stokes parameters). Figure 3 shows the resulting streamwise velocities (i.e., velocity components parallel to oscillation direction of the cylinder) as a function of r at $\theta=0$ and $\pi/2$, for flows with $\beta=1$ and 10; r and θ are the radial and azimuth coordinates of the polar coordinate system. We do not show numerical results for $\beta=5$ since this exhibits similar features to the other values of β. For clarity, data in Fig. 3 are plotted on a logarithmic scale and results beyond a distance of $30a$ are not shown because they are negligibly small. As expected, fluid velocities decay as r increases and tend to zero at large distances from the cylinder. It is also observed that fluid velocities at different azimuthal coordinates have an identical decay rate with respect to the Stokes

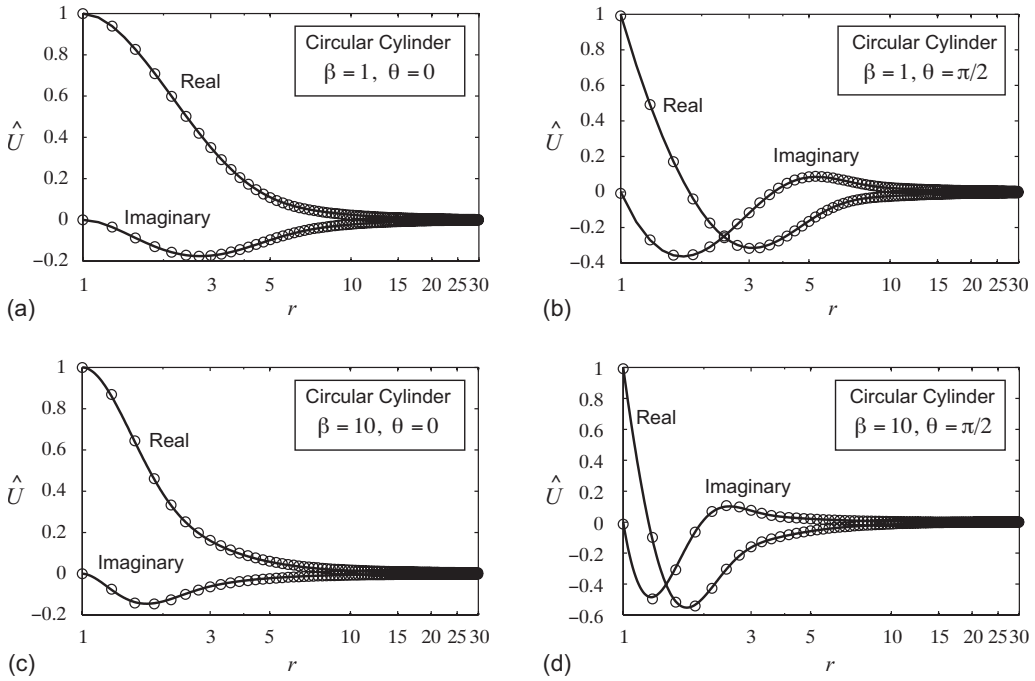

FIG. 3. Dimensionless streamwise velocities in two-dimensional flow around an oscillating circular cylinder. Open circles: numerical results; solid lines: analytical solution.

parameter, β. Namely, flows with larger Stokes parameter β always exhibit faster decay rates. This is expected, since the Stokes parameter β is proportional to the squared ratio of the characteristic dimensions of the cylinder (radius a) to the viscous penetration depth over which vorticity diffuses [52,53]. Superimposed on these viscous effects, however, is an inviscid component due to the cylinder exhibiting a velocity component normal to its surface. This feature results in a finite decay length as the Stokes parameter approaches infinity, in contrast to the oscillatory Couette flow problem whose decay length approaches zero.

Figure 3 also presents a comparison to the exact analytical solution for this problem, i.e., Eqs. (C5)–(C8). Again, we note that the numerical results obtained by the proposed linear lattice Boltzmann method are in excellent agreement with these analytical solutions. Table II provides further verification for the accuracy of the proposed LB method, where hydrodynamic forces are compared to those given by the exact solution in Eq. (C9). It is found that the relative numerical error in the force is less than 1.1%. Taken together with the results of the previous section, this comparison demonstrates that (i) the proposed LB method can accurately simulate flows in both one and two dimensions and (ii) it easily accommodates flows with either simple or complex boundaries (as in the circular interface on a rectangular grid here).

TABLE II. Dimensionless force per unit length in two-dimensional flow around an oscillating circular cylinder.

	$\mathrm{Re}(\hat{F})$		$\mathrm{Im}(\hat{F})$	
$\beta=\omega a^2/\nu$	Numerical	Analytical	Numerical	Analytical
1	−14.1903	−14.3463	−12.3305	−12.4659
5	−5.0956	−5.1423	−7.1416	−7.1750
10	−3.4030	−3.4056	−5.9765	−5.9754

3. Three-dimensional flow around an oscillating sphere

Finally, we examine the applicability of the proposed LB method to a three-dimensional flow. Specifically, we consider the flow generated by an oscillating sphere of radius a immersed in an unbounded viscous fluid. The sphere oscillates horizontally with velocity $u=u_0e^{i\omega t}$, thus driving the surrounding fluid. In the linear limit of infinitesimal oscillation amplitude, i.e., when the oscillation amplitude is much smaller than the sphere radius a, the flow problem can be solved exactly subject to the no-slip boundary condition at the sphere surface [49]. The corresponding exact analytical solution is given in Appendix C, Sec. C 3.

Rather than invoke axisymmetry, we simulate this flow problem in three dimensions on a cubic grid. As such, we use the 15-bit set defined in Eq. (15) for the discrete velocities, together with the corresponding weights in Eq. (21). To nondimensionalize the simulation, we set the sphere radius $a=1$, the reference density $\rho_0=1$, and defined the Stokes parameter as $\beta=a^2\omega/\nu$. The computational domain was systematically increased in size and grid spacing refined to ensure convergence of solution. A domain $20a\times20a\times20a$ was found to be sufficiently large, ensuring that the fluid velocity at its outer boundary is negligible small and could be safely set to zero. Simulations were performed on a $100\times100\times100$ mesh and employed the same boundary treatment and force evaluation method as for flow around the oscillating circular cylinder, but in three dimensions.

We performed numerical simulations for flows with $\beta=5$, 7.5, and 10. Figure 4 shows the streamwise velocities as

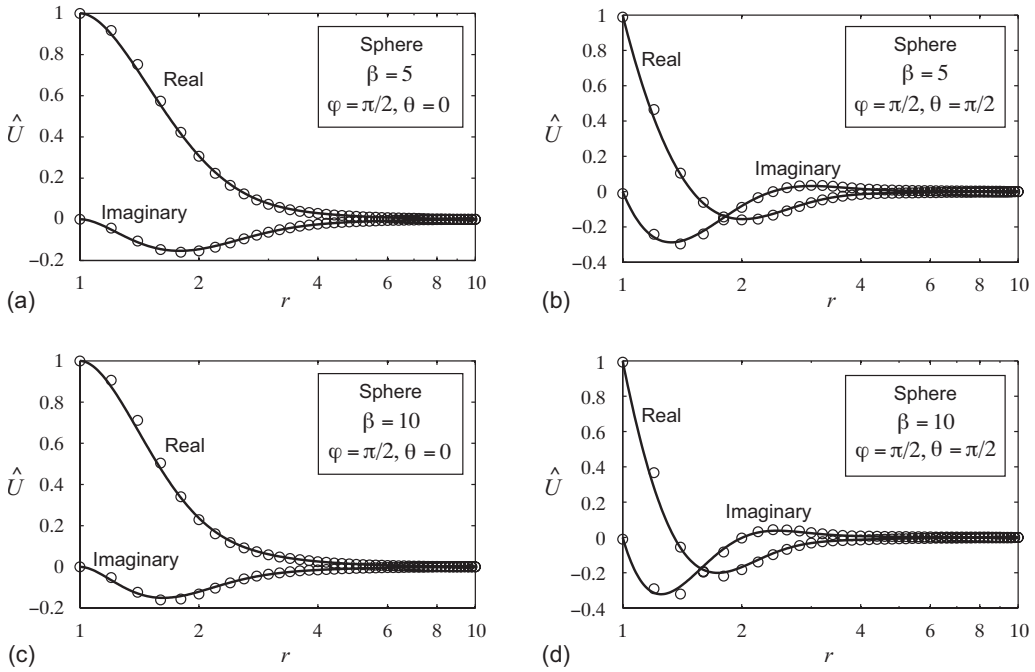

FIG. 4. Dimensionless streamwise velocities in three-dimensional flow around an oscillating sphere. Open circles: numerical results; solid lines: analytical solution.

a function of r at $(\varphi=\pi/2,\ \theta=0)$ and $(\varphi=\pi/2,\ \theta=\pi/2)$ when $\beta=5$ and 10; r, φ, and θ are the usual radial distance and polar and azimuthal angles in spherical coordinate system (see Appendix C, Sec. C 3). Similar to the two-dimensional flow around a circular cylinder in Sec IV A 2, fluid velocities decay as r increases and flows with larger β always decay at a faster rate. Note that we do not present numerical results for $\beta=7.5$, since they exhibit similar behavior and agreement with the exact solution.

Figure 4 shows a direct comparison to the exact analytical solution for the velocity field given in Appendix C, whereas Table III provides a comparison of the forces for $\beta=5$, 7.5, and 10. Note the good agreement throughout, despite the relative coarse grid used (see Fig. 4). The weaker agreement observed here in comparison to the above cases is due to use of a coarser grid. Accuracy can be further improved by use of a finer mesh in the flow region near the sphere surface. However, with the available computing power (Dell OptiPlex 960 Desktop with Intel Core™2 Quad Processors) without parallelization, this would result in an unacceptable computational time for this three-dimensional flow. Use of a nonuniform grid based LB model could also allow for improved computational performance and accuracy.

TABLE III. Dimensionless force generated by three-dimensional flow around an oscillating sphere.

	$\mathrm{Re}(\hat{F})$		$\mathrm{Im}(\hat{F})$	
$\beta=\omega a^2/\nu$	Numerical	Analytical	Numerical	Analytical
5	−9.7590	−9.7307	−8.1883	−8.0551
7.5	−7.4340	−7.3802	−7.1411	−6.9613
10	−6.1691	−6.0998	−6.5060	−6.3093

The excellent agreement in Fig. 4 and Table III validates the proposed LB method for three-dimensional flows. It also demonstrates the applicability of the proposed LB method to general unsteady Stokes flows with complex geometries in three dimensions. This method can also be used to simulate steady Stokes flows in three dimensions, since the Stokes paradox manifests itself only in dimensions less than three [53].

B. Comparison of computational convergence

In Sec. IV A, numerical validations using three classical flow problems were presented, demonstrating the accuracy and applicability of the proposed LB method for oscillatory (unsteady) Stokes flows. Next, we assess its numerical convergence by direct comparison to the conventional time-dependent LB method. Specifically, we consider the two-dimensional unsteady Stokes flow generated around an oscillating infinitely thin blade. This problem finds numerous applications in MEMS and NEMS devices [54–60] and thus its investigation is of intrinsic interest to modern device technologies. Note that this limiting case of an infinitely thin blade can accurately model the practical case of a blade with finite thickness. For a discussion of this pertinent point, see Ref. [54].

Consider an infinitely thin blade of width L immersed in an unbounded viscous fluid with kinematic viscosity ν. The blade oscillates in the direction normal to its plane with a velocity $u=u_0e^{i\omega t}$. The no-slip boundary condition is again applied to the fluid in contact with the blade surface. Since the flow is two dimensional, Eq. (14) was used together with Eq. (20) as the underlying discrete particle velocities and weights in simulations. Nondimensionalization was achieved in the simulation by setting $L=1$, $u_0=0.1$, $\omega=1$, the reference

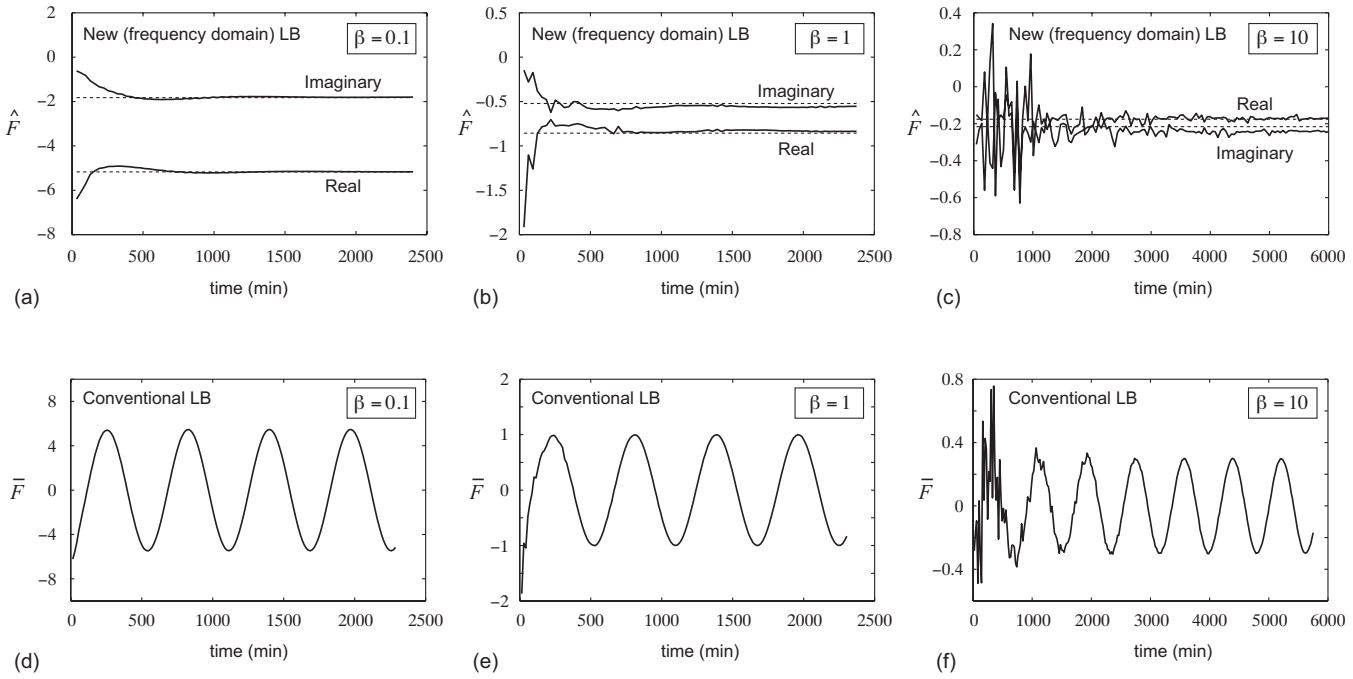

FIG. 5. Dimensionless forces in two-dimensional flow generated by an oscillating infinitely thin flat blade. In (a)–(c), force ($\hat{F}$) is obtained using the frequency domain proposed LB method. Solid line: numerical results; dashed line: exact analytical solution. In (d)–(f), force ($\bar{F}$) is obtained using the conventional time-dependent LB method.

density $\rho_0=1$ and the time step $\Delta t=\Delta\tau=1.571\times10^{-4}$, and the Stokes parameter was defined $\beta=L^2\omega/\nu$. The computation domain was again systematically increased to ensure that the fluid velocity far from the oscillating blade had decayed to zero; a domain of $55L\times55.1L$ was found to be sufficient and used in simulations. The grid spacing was also systematically varied to ensure convergence: a 550×551 mesh was used for flows with small Stokes parameters, while a 660×661 mesh was used for flows with large values ($\beta=10$). The boundary treatment and force evaluation are identical to those used for a circular cylinder (see Sec. IV A 2). Note that a 550×551 (660×661) mesh, rather than 550×550 (660×660), was used in the frequency-domain calculations so that the infinitely thin blade could be placed halfway between two neighboring mesh rows. This ensured the corresponding bounce-back based boundary treatment was accurate to second order [61].

Figures 5(a)–5(c) give the force exerted by the fluid on the blade (as a function of computational time) obtained using the proposed frequency-domain linear LB method for $\beta=0.1$, 1, and 10. In contrast to numerical results presented in Sec. IV A, we now provide the simulation history by presenting numerical results at regular intervals of 1000 iterations in the LB scheme. We remind the reader that the time-marching algorithm is also used in our proposed LB method, but in virtual time τ. It is evident that in all three cases, the resulting complex forces (both real and imaginary parts) exhibit an initial transient response that decays rapidly toward the final converged result. Figures 5(a)–5(c) also present a direct comparison to the exact analytical solutions [62]. The converged complex-valued forces obtained in the simulations are in good agreement with the analytical solutions for all small Stokes parameters β. A small, while still acceptable deviation is observed in Fig. 5(c) when β is increased to 10. This is mainly caused by numerical issues in handling the expected square-root stress singularity at the edge of flat blade, while calculating the force; the importance of this singularity grows as the Stokes parameter increases.

In Figs. 5(d)–5(f), we present complementary results using the conventional time-dependent nonlinear LB method; numerical settings are identical to those used in Figs. 5(a)–5(c) (see above for details). In contrast to the results in Figs. 5(a)–5(c), however, the forces here oscillate periodically with time, consistent with the applied periodic oscillatory motion of the blade. Note that the converged results obtained using two LB methods yield identical results for the forces, i.e., the force magnitude and phase. However, frequency-domain information is often required in applications, necessitating additional numerical processing of the time-dependent force. As such, the direct frequency-domain LB method presents a distinct advantage.

Furthermore, convergence of the (complex-valued) force in the frequency domain is easily recognized, since the result asymptotes to a constant value. This facilitates the minimization of computational time. In contrast, convergence of the conventional time-dependent lattice Boltzmann method necessitates comparison to a (time-varying) sinusoidal function at "large time." As such, convergence cannot be established until several cycles of oscillation have been computed. This increases the computational time in comparison to the direct frequency-domain calculation.

To illustrate this pertinent point, we divided every period in the time-domain simulation into 40 discrete intervals, each of which corresponds to 1000 iterations of the LB method.

This discretization is necessary to ensure that the periodic nature of the force is accurately captured. Importantly, only when all iterations at these 40 discrete intervals have fully converged can one period be compared to another to determine the (long-time) steady-state solution. This requirement contrasts to the simple convergence criterion of the proposed frequency-domain LB method. Importantly, it is the frequency-domain performance that is often required in development and application of MEMS and NEMS.

Finally, we examine the stability of the proposed LB method in comparison to the conventional method. For the flow with $\beta=10$, we performed simulations using the conventional time-domain LB method on the 550×551 mesh discussed above. It was found that the conventional LB method suffered from severe instability and diverged after several thousands iterations. However, by refining the grid further to 660×661, a stable steady state was reached. The reason for this instability is that the dimensionless relaxation frequency, Ω, in the simulation equals 1.981 and is thus very close to the singular limit of $\Omega=2$ [63]. Importantly, such numerical instability did not occur while using the proposed frequency-domain linear LB method with identical Ω and the coarser 550×551 mesh. Simulations demonstrate that the proposed linear LB method converged to its stable steady-state result after only a few initial fluctuations at early iteration. It is known that the inherent nonlinearity in the conventional equilibrium distribution function is the primary factor behind numerical instability when Ω approaches 2 [63]. We therefore attribute this improvement in numerical stability in the proposed LB method to use of the linearized equilibrium distribution function.

C. Discussion

Numerical simulation of the four (linear) unsteady Stokes flows, together with the theoretical analysis in Sec. III, clearly demonstrates that the proposed LB method has a rigorous mathematical basis and exhibits accurate and efficient numerical performance. Specifically, the proposed method improves upon the conventional time-dependent LB method in the following respects:

(1) The proposed LB method is derived directly from the linearized Boltzmann BGK equation and has been proved to be macroscopically equivalent to the linearized Navier-Stokes equations. Compared to the conventional LB method, the proposed linear method exhibits a much simpler equilibrium distribution function and intrinsically excludes the redundant macroscopic nonlinear advection term from simulations—this is the practical case in many small-scale flows.

(2) The proposed LB method is formulated in the frequency-domain, enabling direct access to the frequency response of the fluid flow, which is of fundamental interest in many practical applications involving MEMS and NEMS technologies. A direct consequence is that the proposed LB method directly outputs time-independent variables for oscillatory flows, instead of periodically varying time-dependent solutions. This enables rapid convergence recognition and improved numerical efficiency, in comparison to the conventional LB method.

(3) Unlike the conventional LB method, the proposed LB method obviates the need for tracking the movement of solid boundaries at every time step since the original time-varying boundaries are transformed into fixed boundaries in the frequency domain. The proposed LB method thus employs identical boundary treatments to the conventional LB method with fixed boundaries. This facilitates compact coding and improves computational efficiency.

(4) Due to its inherent linearity, the proposed LB method can also employ direct computational solvers based on established linear algebra techniques. This would eliminate the need for time-consuming iterative algorithms, such as the conventional time-marching scheme that has been employed here. Such a solver has the potential to greatly improve computational efficiency and speed. Even so, it must be noted that such an improvement comes at the cost of not allowing for compatibility with existing LB programs and hence has not been explored here. This algorithmic improvement will be discussed in future work.

V. CONCLUSIONS

In this paper, we proposed a lattice Boltzmann method for linear oscillatory Stokes flows. In comparison to the conventional lattice Boltzmann method, the proposed method presents a number of distinct improvements. First, the method is based on the linearized Boltzmann BGK equation so that the nonlinear advective inertial effect is explicitly removed. This makes it directly applicable to micro- and nanoscale flows and circumvents stability issues inherent in the conventional nonlinear method. Moreover, the proposed LB method is derived in the frequency domain, rather than in the conventional time domain, enabling direct computation of the more practically relevant frequency response. From a numerical and computational perspective, the proposed LB method retains the original time-marching structure through introduction of a "virtual time." This makes it completely compatible with all existing time-dependent lattice Boltzmann programs.

Validity and accuracy of the proposed method were assessed by comparison to three classical flow problems studied by Stokes (1901). The excellent quantitative agreement in all cases demonstrates that the proposed method is an accurate and effective numerical approach for oscillatory Stokes flows of any dimensionality. As with conventional LB method, it can also easily handle geometries of complex shape. Consequently, the proposed LB method provides a robust and effective computational tool for future developments in MEMS and NEMS technologies.

ACKNOWLEDGMENTS

Y.S. would like to acknowledge partial support from NSFC (Grants No. 50806085 and No. 90510020). The authors gratefully acknowledge support from the Australian Research Council Grants Scheme.

APPENDIX A: RECOVERING THE LINEARIZED NAVIER-STOKES EQUATIONS THROUGH THE CHAPMAN-ENSKOG PROCEDURE

In this appendix, we derive the linearized Navier-Stokes equations based on the linearized Boltzmann BGK equation,

Eq. (11), through the Chapman-Enskog procedure. We first present the following multiscale expansion:

$$h = (-1) + M^{(0)} + \mathrm{Kn}\, M^{(1)} + \mathrm{Kn}^2\, M^{(2)} + \cdots, \quad \text{(A1)}$$

$$\frac{\partial}{\partial t} = \mathrm{Kn}\frac{\partial_1}{\partial t} + \mathrm{Kn}^2\frac{\partial_2}{\partial t}, \quad \text{(A2)}$$

$$\frac{\partial}{\partial \mathbf{r}} = \mathrm{Kn}\frac{\partial_1}{\partial \mathbf{r}}, \quad \text{(A3)}$$

where $M^{(i)}=f^{(i)}/\bar{f}^{eq}$ and $f^{(i)}$ is the ith order term in the multiscale expansion of f, Kn is Knudsen number defined as a ratio of the molecular dimension to the macroscopic length scale, and $\partial_1/\partial t$ and $\partial_2/\partial t$ are derivatives at the convection and diffusion time scales, respectively. Substituting the expansions in Eqs. (A1)–(A3) into Eq. (11), we obtain the following set of equations in different orders of Knudsen number:

$$\mathrm{Kn}^0: \quad M^{(0)} = \frac{f_L^{eq}}{\bar{f}^{eq}}, \quad \text{(A4)}$$

$$\mathrm{Kn}^1: \quad \frac{\partial_1}{\partial t}M'^{(0)} + \mathbf{c}\cdot\frac{\partial_1}{\partial \mathbf{r}}M'^{(0)} = -\frac{1}{\lambda}M^{(1)}, \quad \text{(A5)}$$

$$\mathrm{Kn}^2: \quad \frac{\partial_1}{\partial t}M^{(1)} + \frac{\partial_2}{\partial t}M'^{(0)} + \mathbf{c}\cdot\frac{\partial_1}{\partial \mathbf{r}}M^{(1)} = -\frac{1}{\lambda}M^{(2)}, \quad \text{(A6)}$$

where $M'^{(0)}=M^{(0)}-1$. Furthermore, with the help of Eqs. (6) and (7) and the definitions of f_L^{eq} and $\bar{f}^{eq}$, we obtain the moments

$$\int \bar{f}^{eq}M'^{(0)}d\mathbf{c} = \delta\rho, \quad \int \bar{f}^{eq}M^{(r)}d\mathbf{c} = 0 \quad \text{for} \quad r = 1,2,\ldots, \quad \text{(A7)}$$

$$\int \bar{f}^{eq}M'^{(0)}\mathbf{c}d\mathbf{c} = \rho_0\mathbf{u}, \quad \int \bar{f}^{eq}M^{(r)}\mathbf{c}d\mathbf{c} = \mathbf{0},$$

for

$$r = 1,2,\ldots, \quad \text{(A8)}$$

$$\int \bar{f}^{eq}M'^{(0)}\mathbf{c}\mathbf{c}d\mathbf{c} = \delta p\mathbf{I}, \quad \text{(A9)}$$

where $\delta p=\delta\rho RT_0$ and $\mathbf{I}$ is the unity tensor of second rank.

Multiplying both the sides of Eq. (A5) by $\{\bar{f}^{eq},\bar{f}^{eq}\mathbf{c}\}$, integrating over the entire particle velocity space, and using Eqs. (A7)–(A9), we obtain the macroscopic mass and momentum conservation equations to linear order in Kn, respectively,

$$\frac{\partial_1}{\partial t}\delta\rho + \frac{\partial_1}{\partial \mathbf{r}}\cdot(\rho_0\mathbf{u}) = 0, \quad \text{(A10)}$$

$$\frac{\partial_1}{\partial t}(\rho_0\mathbf{u}) + \frac{\partial_1}{\partial \mathbf{r}}\delta p = 0. \quad \text{(A11)}$$

From Eqs. (A5) and (A10), we also have

$$\int \bar{f}^{eq}M^{(1)}\mathbf{c}\mathbf{c}d\mathbf{c} = -\lambda\rho_0 RT_0\left[\frac{\partial_1}{\partial \mathbf{r}}\mathbf{u} + \left(\frac{\partial_1}{\partial \mathbf{r}}\mathbf{u}\right)^T\right], \quad \text{(A12)}$$

where the superscript T denotes the transpose.

Similarly, we derive the macroscopic mass and momentum conservation equations to second order in Kn, based on Eq. (A6). Using Eq. (A12), we obtain

$$\frac{\partial_2}{\partial t}\delta\rho = 0, \quad \text{(A13)}$$

$$\frac{\partial_2}{\partial t}(\rho_0\mathbf{u}) = \frac{\partial_1}{\partial \mathbf{r}}\cdot\left\{\mu\left[\frac{\partial_1}{\partial \mathbf{r}}\mathbf{u} + \left(\frac{\partial_1}{\partial \mathbf{r}}\mathbf{u}\right)^T\right]\right\}, \quad \text{(A14)}$$

where the viscosity $\mu=\lambda\rho_0 RT_0$.

Finally, combining Eqs. (A10) and (A11) with Eqs. (A13) and (A14), respectively, we obtain

$$\frac{\partial}{\partial t}\delta\rho + \frac{\partial}{\partial \mathbf{r}}\cdot(\rho_0\mathbf{u}) = 0, \quad \text{(A15)}$$

$$\frac{\partial}{\partial t}(\rho_0\mathbf{u}) = -\frac{\partial}{\partial \mathbf{r}}\delta p + \frac{\partial}{\partial \mathbf{r}}\cdot\left\{\mu\left[\frac{\partial}{\partial \mathbf{r}}\mathbf{u} + \left(\frac{\partial}{\partial \mathbf{r}}\mathbf{u}\right)^T\right]\right\}. \quad \text{(A16)}$$

Equations (A15) and (A16) clearly reduce to the incompressible linearized Navier-Stokes equations in the incompressible limit.

APPENDIX B: RECOVERING THE LINEARIZED NAVIER-STOKES EQUATIONS IN THE FREQUENCY DOMAIN FROM THE LINEARIZED LATTICE BOLTZMANN BGK METHOD

Here, we derive the macroscopic governing equations from the linear lattice Boltzmann BGK method using the Chapman-Enskog procedure. We first expand $\hat{h}_j(\mathbf{r}+\mathbf{c}_j\Delta\tau,\tau+\Delta\tau)$ in its Taylor series about $\mathbf{r}$ and τ. Substituting the resulting expansion into Eq. (28) gives

$$\frac{\partial\hat{h}_j}{\partial\tau} + \mathbf{c}_j\cdot\frac{\partial\hat{h}_j}{\partial\mathbf{r}} + \frac{\Delta\tau}{2}\left[\frac{\partial^2\hat{h}_j}{\partial\tau^2} + 2\mathbf{c}_j\cdot\frac{\partial}{\partial\mathbf{r}}\left(\frac{\partial\hat{h}_j}{\partial\tau}\right) + \mathbf{c}_j\mathbf{c}_j:\frac{\partial}{\partial\mathbf{r}}\left(\frac{\partial\hat{h}_j}{\partial\mathbf{r}}\right)\right] = -\frac{\hat{h}_j}{\lambda^*} + \frac{\hat{h}_j^{eq}}{\lambda} - \frac{\Delta\tau}{2}\omega^2\hat{h}_j^{eq}. \quad \text{(B1)}$$

Next, we present the multiscale expansions

$$\hat{h}_j = \hat{h}_j^{(0)} + \mathrm{Kn}\,\hat{h}_j^{(1)} + \mathrm{Kn}^2\,\hat{h}_j^{(2)} + \cdots, \quad \text{(B2)}$$

$$\frac{\partial}{\partial\tau} = \mathrm{Kn}\frac{\partial_1}{\partial\tau} + \mathrm{Kn}^2\frac{\partial_2}{\partial\tau}, \quad \text{(B3)}$$

$$\omega = \mathrm{Kn}\,\omega_1 + \mathrm{Kn}^2\,\omega_2, \quad \text{(B4)}$$

and

$$\frac{\partial}{\partial \mathbf{r}} = \mathrm{Kn}\frac{\partial_1}{\partial \mathbf{r}}. \tag{B5}$$

Using Eqs. (B2)–(B5), we rewrite Eq. (B1) as a series of equations at different orders in Kn,

$$\mathrm{Kn}^0: \quad \hat{h}_j^{(0)} = \hat{h}_j^{eq}, \tag{B6}$$

$$\mathrm{Kn}^1: \quad \frac{\partial_1}{\partial \tau}\hat{h}_j^{(0)} + \mathbf{c}_j \cdot \frac{\partial_1}{\partial \mathbf{r}}\hat{h}_j^{(0)} = -\frac{1}{\lambda}\hat{h}_j^{(1)} - i\omega_1 \hat{h}_j^{(0)}, \tag{B7}$$

$$\begin{aligned}\mathrm{Kn}^2: \quad & \frac{\partial_2}{\partial \tau}\hat{h}_j^{(0)} + \frac{\partial_1}{\partial \tau}\hat{h}_j^{(1)} + \mathbf{c}_j \cdot \frac{\partial_1 \hat{h}_j^{(1)}}{\partial \mathbf{r}} \\ & + \frac{\Delta\tau}{2}\left[\frac{\partial_1^2 \hat{h}_j^{(0)}}{\partial \tau^2} + 2\mathbf{c}_j \cdot \frac{\partial_1}{\partial \mathbf{r}}\left(\frac{\partial_1 \hat{h}_j^{(0)}}{\partial \tau}\right) + \mathbf{c}_j\mathbf{c}_j : \frac{\partial_1}{\partial \mathbf{r}}\left(\frac{\partial_1 \hat{h}_j^{(0)}}{\partial \mathbf{r}}\right)\right] \\ & = -\frac{1}{\lambda}\hat{h}_j^{(2)} - i\omega_1 \hat{h}_j^{(1)} - i\omega_2 \hat{h}_j^{(0)} - \frac{\Delta\tau}{2}\omega_1^2 \hat{h}_j^{(eq)}.\end{aligned} \tag{B8}$$

Note that based on Eqs. (B6) and (B7), Eq. (B8) can be further reduced to

$$\begin{aligned}\mathrm{Kn}^2: \quad & \frac{\partial_2}{\partial \tau}\hat{h}_j^{(0)} + \left(1 - \frac{\Delta\tau}{2\lambda}\right)\left(\frac{\partial_1}{\partial \tau}\hat{h}_j^{(1)} + \mathbf{c}_j \cdot \frac{\partial_1 \hat{h}_j^{(1)}}{\partial \mathbf{r}}\right) \\ & - \frac{\Delta\tau}{2} i\omega_1 \left(\frac{\partial_1}{\partial \tau}\hat{h}_j^{(0)} + \mathbf{c}_j \cdot \frac{\partial_1 \hat{h}_j^{(0)}}{\partial \mathbf{r}}\right) \\ & = -\frac{1}{\lambda}\hat{h}_j^{(2)} - i\omega_1 \hat{h}_j^{(1)} - i\omega_2 \hat{h}_j^{(0)} - \frac{\Delta\tau}{2}\omega_1^2 \hat{h}_j^{(0)}.\end{aligned} \tag{B9}$$

On the other hand, based on Eqs. (B6), (25), and (26), we have the following quadratures for different orders of $\hat{h}_j^{(n)}$:

$$\sum_j \rho_0 w_j \hat{h}_j^{(0)} = \delta\hat{\rho}, \quad \sum_j \rho_0 w_j \hat{h}_j^{(n)} = 0, \quad \text{for} \quad (n > 0), \tag{B10}$$

$$\sum_j w_j \hat{h}_j^{(0)} \mathbf{c}_j = \hat{\mathbf{u}}, \quad \sum_j w_j \hat{h}_j^{(n)} \mathbf{c}_j = \mathbf{0}, \quad \text{for} \quad (n > 0), \tag{B11}$$

$$\sum_j \rho_0 w_j \hat{h}_j^{(0)} \mathbf{c}_j \mathbf{c}_j = \delta\hat{p}\mathbf{I}. \tag{B12}$$

By multiplying both the sides of Eq. (B7) by $\{w_j\rho_0, \ \rho_0 w_j \mathbf{c}_j\}$ and summing over all discrete particle velocity space, we obtain the mass and momentum equations to linear order in Kn,

$$\frac{\partial_1}{\partial \tau}(\delta\hat{\rho}) + \frac{\partial_1}{\partial \mathbf{r}} \cdot (\rho_0 \hat{\mathbf{u}}) = -i\omega_1 \delta\hat{\rho}, \tag{B13}$$

$$\frac{\partial_1(\rho_0 \hat{\mathbf{u}})}{\partial \tau} = -\frac{\partial_1}{\partial \mathbf{r}}\delta\hat{p} - i\omega_1 \rho_0 \hat{\mathbf{u}}. \tag{B14}$$

Further, we also have

$$\sum_j \rho_0 w_j \hat{h}_j^{(1)} \mathbf{c}_j \mathbf{c}_j = (-\lambda)\rho_0 c_s^2 \left[\frac{\partial_1}{\partial \mathbf{r}}\hat{\mathbf{u}} + \left(\frac{\partial_1}{\partial \mathbf{r}}\hat{\mathbf{u}}\right)^T\right]. \tag{B15}$$

Similarly, we multiply both the sides of Eq. (B9) by $\{w_j\rho_0, \ \rho_0 w_j \mathbf{c}_j\}$ and sum over all discrete particle velocity spaces. Using Eqs. (B10)–(B15), we obtain the mass and momentum equations to order Kn^2,

$$\frac{\partial_2}{\partial \tau}(\delta\hat{\rho}) = -i\omega_2 \delta\hat{\rho}, \tag{B16}$$

$$\frac{\partial_2}{\partial \tau}(\rho_0 \hat{\mathbf{u}}) = -i\omega_2 \rho_0 \hat{\mathbf{u}} + \mu\left(\frac{\partial_1}{\partial \mathbf{r}} \cdot \left[\frac{\partial_1}{\partial \mathbf{r}}\hat{\mathbf{u}} + \left(\frac{\partial_1}{\partial \mathbf{r}}\hat{\mathbf{u}}\right)^T\right]\right), \tag{B17}$$

with viscosity $\mu = \Delta\tau\rho_0 c_s^2(1/\Omega - 1/2)$.

Combining Eqs. (B13) and (B14) with Eqs. (B16) and (B17), respectively, we obtain

$$\frac{\partial}{\partial \tau}(\delta\hat{\rho}) + \frac{\partial}{\partial \mathbf{r}} \cdot (\rho_0 \hat{\mathbf{u}}) = -i\omega\delta\hat{\rho}, \tag{B18}$$

$$\frac{\partial(\rho_0 \hat{\mathbf{u}})}{\partial \tau} = -\frac{\partial}{\partial \mathbf{r}}\delta\hat{p} + \mu\left(\frac{\partial}{\partial \mathbf{r}} \cdot \left[\frac{\partial}{\partial \mathbf{r}}\hat{\mathbf{u}} + \left(\frac{\partial}{\partial \mathbf{r}}\hat{\mathbf{u}}\right)^T\right]\right) - i\omega\rho_0 \hat{\mathbf{u}}. \tag{B19}$$

Clearly, in the steady-state case, Eqs. (B18) and (B19) reduce to the linearized Navier-Stokes equations in the frequency domain

$$i\omega\delta\hat{\rho} + \frac{\partial}{\partial \mathbf{r}} \cdot (\rho_0 \hat{\mathbf{u}}) = 0, \tag{B20}$$

$$i\omega\rho_0 \hat{\mathbf{u}} = -\frac{\partial}{\partial \mathbf{r}}\delta\hat{p} + \mu\left(\frac{\partial}{\partial \mathbf{r}} \cdot \left[\frac{\partial}{\partial \mathbf{r}}\hat{\mathbf{u}} + \left(\frac{\partial}{\partial \mathbf{r}}\hat{\mathbf{u}}\right)^T\right]\right). \tag{B21}$$

This is the required result and establishes that the proposed LB method is formally equivalent to the linearized Navier-Stokes equations.

APPENDIX C: ANALYTICAL SOLUTIONS OF CLASSICAL OSCILLATORY FLOW PROBLEMS

We now present analytical solutions to the classical flow problems studied in Sec. IV A. Since we are primarily interested in the frequency response of flows to the applied oscillatory motion, analytical solutions are given in the frequency domain.

1. One-dimensional oscillatory Couette flow

We first consider one-dimensional oscillatory Couette flow [Fig. 1(a)], where the bottom plate is oscillating and the top plate is stationary. As presented in Sec. IV A 1, such a flow is driven by the bottom oscillatory plate and described by the linearized Navier-Stokes equations. The fluid velocity can be solved analytically to obtain

$$\hat{U} = a_1 e^{\sqrt{i\beta}Y} + a_2 e^{-\sqrt{i\beta}Y}, \tag{C1}$$

where Y is the dimensionless coordinate in the direction normal to the plate, scaled by L, and $\hat{U}$ is the scaled streamwise velocity (parallel to the plate) in the frequency domain, scaled by u_0, The coefficients in Eq. (C1) are

$$a_1 = -e^{-\sqrt{i\beta}}/[2\sinh(\sqrt{i\beta})], \tag{C2}$$

$$a_2 = e^{\sqrt{i\beta}}/[2\sinh(\sqrt{i\beta})], \tag{C3}$$

where the Stokes parameter $\beta = \omega L^2/\nu$. The scaled shear stress on the bottom oscillating plate can also be evaluated

$$\hat{F} = -\frac{\sqrt{i\beta}\coth(\sqrt{i\beta})}{\beta}, \tag{C4}$$

where it is scaled by $\rho u_0 L\omega$.

2. Two-dimensional flow around an oscillating cylinder

The flow generated by an oscillating circular cylinder [Fig. 1(b)] can be described by the linearized Navier-Stokes equations in cylindrical coordinates when the spatial amplitude of the oscillation is be much smaller than the characteristic length of flow (the radius of the cylinder a). The corresponding analytical solutions are [50]

$$\hat{v}_r = \frac{A\cos\theta}{r^2} + \frac{B\cos\theta}{r}K_1(r\sqrt{i\beta}), \tag{C5}$$

$$\hat{v}_\theta = \frac{A\sin\theta}{r^2} - B\sin\theta\sqrt{i\beta}K_1'(r\sqrt{i\beta}), \tag{C6}$$

where θ is the azimuthal coordinate, r is the radial distance scaled by a, the Stokes parameter $\beta = \omega a^2/\nu$, and $\hat{v}_r$ and $\hat{v}_\theta$ are the dimensionless velocity components in the radial and circumferential directions in the frequency domain, respectively. Both of these velocities are scaled by u_0. In Eqs. (C5) and (C6), the coefficients A and B are

$$A = 1 + 2K_1(\sqrt{i\beta})/[\sqrt{i\beta}K_0(\sqrt{i\beta})], \tag{C7}$$

$$B = -2/[\sqrt{i\beta}K_0(\sqrt{i\beta})], \tag{C8}$$

where $K_0(z)$ and $K_1(z)$ are modified Bessel functions of the third kind [64]. In this flow, the scaled force exerted by the fluid on the surface of the cylinder is

$$\hat{F} = -\pi i\{1 - 4K_1(\sqrt{i\beta})/[K_1(\sqrt{i\beta}) + \sqrt{i\beta}K_1'(\sqrt{i\beta})]\}, \tag{C9}$$

where $\hat{F}$ is the force on per unit length of the cylinder defined in the frequency domain, scaled by $\rho a^2 u_0 \omega$.

3. Three-dimensional flow around an oscillating sphere

Three-dimensional flow around a sphere of radius a oscillating horizontally with a velocity $u = u_0 e^{i\omega t}$ is now analyzed (see Fig. 1(c)). When the spatial amplitude of the oscillation is very small in comparison to a, the analytical solution for the fluid velocity is

$$\hat{v}_r = \frac{f'\cos\theta\cos\varphi\cot\varphi}{r} - \frac{f'\cos\theta\sin\varphi}{r} - \frac{f'\cos\theta}{r\sin\varphi}, \tag{C10}$$

$$\hat{v}_\varphi = -\frac{f'\cos\theta\cos\varphi}{r} - f''\cos\theta\cos\varphi, \tag{C11}$$

$$\hat{v}_\theta = \frac{f'\sin\theta}{r} + f''\sin\theta, \tag{C12}$$

where r, φ, and θ denote the radial distance and polar and azimuthal angles in the spherical coordinates, respectively, $\hat{v}_r$, $\hat{v}_\varphi$, and $\hat{v}_\theta$ are the corresponding velocity components in these directions defined in the frequency domain. Note that in Eqs. (C10)–(C12), r is scaled by a, while $\{\hat{v}_r, \hat{v}_\varphi, \hat{v}_\theta\}$ are scaled by u_0. The functions $f'(r)$ and $f''(r)$ are given by

$$f'(r) = \frac{Ae^{-r\sqrt{i\beta}}(r + 1/\sqrt{i\beta}) + B}{r^2}, \tag{C13}$$

$$f''(r) = -\frac{A\sqrt{i\beta}e^{-r\sqrt{i\beta}} + 2f'(r)}{r}, \tag{C14}$$

where $\beta = \omega a^2/\nu$ and

$$A = 3e^{\sqrt{i\beta}}/(2\sqrt{i\beta}), \tag{C15}$$

$$B = -\frac{1}{2}[1 + 3/\sqrt{i\beta} + 3/(i\beta)]. \tag{C16}$$

The scaled force on the sphere exerted by the fluid on the sphere is [50]

$$\hat{F} = -\frac{4\pi}{3}i[k - ik'], \tag{C17}$$

which has been scaled by $\rho a^3 u_0 \omega$

$$k = \frac{1}{2} + \frac{9}{4}\sqrt{\frac{2}{\beta}}, \tag{C18}$$

$$k' = \frac{9}{4}\left\{\sqrt{\frac{2}{\beta}} + \frac{2}{\beta}\right\}. \tag{C19}$$

[1] R. Benzi, S. Succi, and M. Vergassola, Phys. Rep. **222**, 145 (1992).
[2] S. Chen and G. D. Doolen, Annu. Rev. Fluid Mech. **30**, 329 (1998).
[3] L.-S. Luo, *The Lattice-Gas and Lattice Boltzmann Methods: Past, Present and Future*, in Proceedings of the International Conference on Applied Computational Fluid Dynamics, Beijing, 2000, edited by J.-H. Wu and Z.-J. Zhu (Beijing, China, 2000) p. 52–83. Available at http://www.lions.odu.edu/~lluo/.
[4] S. Succi, *The Lattice Boltzmann Equation for Fluid Dynamics and Beyond* (Clarendon Press, Oxford, 2001).
[5] X. He and L.-S. Luo, Phys. Rev. E **56**, 6811 (1997).
[6] X. He and G. D. Doolen, J. Stat. Phys. **107**, 309 (2002).
[7] Y. Shi, T. S. Zhao, and Z. L. Guo, Phys. Rev. E **70**, 066310 (2004).
[8] X. Shan and H. Chen, Phys. Rev. E **47**, 1815 (1993).
[9] L.-S. Luo, Phys. Rev. E **62**, 4982 (2000).
[10] O. Filippova and D. Hanel, J. Comput. Phys. **147**, 219 (1998).
[11] Z. Guo, C. Zheng, and B. Shi, Phys. Fluids **14**, 2007 (2002).
[12] D. Yu, R. Mei, L.-S. Luo, and W. Shyy, Prog. Aerosp. Sci. **39**, 329 (2003).
[13] D. R. Noble, J. G. Georgiadis, and R. O. Buckius, Int. J. Numer. Methods Fluids **23**, 1 (1996).
[14] D. Kandhai, A. Koponen, A. G. Hoekstra, M. Kataja, J. Timonen, and P. M. A. Sloot, Comput. Phys. Commun. **111**, 14 (1998).
[15] H. Chen, Y. S. Kandasam, S. Orszag, R. Shock, S. Succi, and V. Yakhot, Science **301**, 633 (2003).
[16] H. Yu, S. S. Girimaji, and L.-S. Luo, J. Comput. Phys. **209**, 599 (2005).
[17] N. S. Martys and H. D. Chen, Phys. Rev. E **53**, 743 (1996).
[18] Q. J. Kang, D. X. Zhang, and S. Y. Chen, Phys. Rev. E **66**, 056307 (2002).
[19] R. R. Nourgaliev, T. N. Dinh, T. G. Theofanous, and D. Joseph, Int. J. Multiphase Flow **29**, 117 (2003).
[20] T. Inamuro, T. Ogata, S. Tajima, and N. Konishi, J. Comput. Phys. **198**, 628 (2004).
[21] S. Y. Chen, H. D. Chen, D. Martinez, and W. Matthaeus, Phys. Rev. Lett. **67**, 3776 (1991).
[22] A. J. C. Ladd, J. Fluid Mech. **271**, 285 (1994).
[23] A. J. C. Ladd, J. Fluid Mech. **271**, 311 (1994).
[24] C. H. Sun, C. Migliorini, and L. L. Munn, Biophys. J. **85**, 208 (2003).
[25] M. M. Dupin, I. Halliday, and C. M. Care, J. Phys. A **36**, 8517 (2003).
[26] M. Wang, J. Wang, N. Pan, and S. Chen, Phys. Rev. E **75**, 036702 (2007).
[27] M. Wang and N. Pan, Mater. Sci. Eng. R. **63**, 1 (2008).
[28] M. Wang and N. Pan, J. Comput. Phys. **228**, 5978 (2009).
[29] D. A. Wolf-Gladrow, *Lattice-Gas Cellular Automata and Lattice Boltzmann Models: An Introduction* (Springer, New York, 2000).
[30] U. Frisch, B. Hasslacher, and Y. Pomeau, Phys. Rev. Lett. **56**, 1505 (1986).
[31] G. R. McNamara and G. Zanetti, Phys. Rev. Lett. **61**, 2332 (1988).
[32] F. J. Higuera and J. Jimenez, Europhys. Lett. **9**, 663 (1989).
[33] F. J. Higuera, S. Succi, and R. Benzi, Europhys. Lett. **9**, 345 (1989).
[34] Y. H. Qian, D. d'Humieres, and P. Lallemand, Europhys. Lett. **17**, 479 (1992).
[35] Y. Shi, T. S. Zhao, and Z. L. Guo, Phys. Rev. E **76**, 016707 (2007).
[36] D. Hlushkou, D. Kandhai, and U. Tallarek, Int. J. Numer. Methods Fluids **46**, 507 (2004).
[37] M. Wang and Q. Kang, Anal. Chem. **81**, 2953 (2009).
[38] Y.-H. Cho, A. P. Pisano, and R. T. Howe, J. Microelectromech. Syst. **3**, 81 (1994).
[39] W. Ye, X. Wang, W. Hemmert, D. Freeman, and J. White, J. Microelectromech. Syst. **12**, 557 (2003).
[40] G. Stemme, J. Micromech. Microeng. **1**, 113 (1991).
[41] C. Ziegler, Anal. Bioanal. Chem. **379**, 946 (2004).
[42] F. Meng, M. Wang, and Z. Li, Int. J. Heat Fluid Flow **29**, 1203 (2008).
[43] M. Maute, S. Raible, F. E. Prins, D. P. Kern, H. Ulmer, U. Weimar, and W. Gopel, Sens. Actuators B **58**, 505 (1999).
[44] M. K. Ghatkesar, V. Barwich, T. Braun, A. H. Bredekamp, U. Drechsler, M. Despont, H. P. Lang, M. Hegner, and C. H. Gerber, Proceedings of IEEE on Sensors **2**, 1060 (2004).
[45] P. S. Waggoner and H. G. Craighead, Lab Chip **7**, 1238 (2007).
[46] P. L. Bhatnagar, E. P. Gross, and M. Krook, Phys. Rev. **94**, 511 (1954).
[47] S. Chapman and T. G. Cowling, *The Mathematical Theory of Non-Uniform Gases: An Account of the Kinetic Theory of Viscosity, Thermal Conduction and Diffusion in Gases* (Cambridge University Press, Cambridge, England, 1990).
[48] C. Cercignani, *Rarefied Gas Dynamics: From Basic Concepts to Actual Calculations* (Cambridge University Press, Cambridge, England, 2000).
[49] G. G. Stokes, *Mathematical and Physical Papers* (Cambridge University Press, Cambridge, England, 1901), Vol. 3.
[50] L. Rosenhead, *Laminar Boundary Layers* (Clarendon Press, Oxford, 1963).
[51] R. Mei, D. Yu, and W. Shyy, Phys. Rev. E **65**, 041203 (2002).
[52] L. D. Landau and E. M. Lifshitz, *Fluid Mechanics* (Pergamon Press, Sydney, 1987).
[53] G. K. Batchelor, *An Introduction to Fluid Dynamics* (Cambridge University Press, London, 1967).
[54] J. E. Sader, J. Appl. Phys. **84**, 64 (1998).
[55] F. Pan, J. Kubby, E. Peeters, A. T. Tran, and S. Mukherjee, J. Micromech. Microeng. **8**, 200 (1998).
[56] A. Pavlov, Y. Pavlova, and R. Laiho, Rev. Adv. Mater. Sci. **5**, 324 (2003).
[57] M. R. Paul and M. C. Cross, Phys. Rev. Lett. **92**, 235501 (2004).
[58] R. J. Clarke, S. M. Cox, P. M. Williams, and O. E. Jensen, J. Fluid Mech. **545**, 397 (2005).
[59] C. P. Green and J. E. Sader, Phys. Fluids **17**, 073102 (2005).
[60] S. Basak, A. Raman, and S. V. Garimella, J. Appl. Phys. **99**, 114906 (2006).
[61] X. He, Q. Zou, L.-S. Luo, and M. Dembo, J. Stat. Phys. **87**, 115 (1997).
[62] C. A. Van Eysden and J. E. Sader, J. Appl. Phys. **101**, 044908 (2007).
[63] J. D. Sterling and S. Chen, J. Comput. Phys. **123**, 196 (1996).
[64] M. Abramowitz and I. A. Stegun, *Handbook of Mathematical Functions* (Dover, New York, 1972).